NANO LETTERS

pubs.acs.org/NanoLett

Low-Temperature Thermoelectric Power Factor Enhancement by Controlling Nanoparticle Size Distribution

Mona Zebarjadi,[†] Keivan Esfarjani,[†,‡] Zhixi Bian,[†] and Ali Shakouri*[,†]

[†]Department of Electrical Engineering and [‡]Department of Physics, University of California, Santa Cruz California 95064, United States

ABSTRACT Coherent potential approximation is used to study the effect of adding doped spherical nanoparticles inside a host matrix on the thermoelectric properties. This takes into account electron multiple scatterings that are important in samples with relatively high volume fraction of nanoparticles (>1%). We show that with large fraction of uniform small size nanoparticles (~1 nm), the power factor can be enhanced significantly. The improvement could be large (up to 450% for GaAs) especially at low temperatures when the mobility is limited by impurity or nanoparticle scattering. The advantage of doping via embedded nanoparticles compared to the conventional shallow impurities is quantified. At the optimum thermoelectric power factor, the electrical conductivity of the nanoparticle-doped material is larger than that of impurity-doped one at the studied temperature range (50−500 K) whereas the Seebeck coefficient of the nanoparticle doped material is enhanced only at low temperatures (~50 K).

KEYWORDS Electrical transport, thermoelectrics, coherent potential approximation, nanoparticles

Thermoelectric power generators are clean, noise free solid-state systems that directly convert heat into electricity. These devices have potential applications in waste heat recovery. The energy conversion efficiency depends on the material's dimensionless thermoelectric figure-of-merit $ZT = \sigma S^2 T/\kappa$, where σ is the electrical conductivity, S is the Seebeck coefficient; T is the operating temperature, and κ is the thermal conductivity.[1] Several recent publications focus on embedding nanoparticles inside semiconductor host materials to improve their thermoelectric properties[2,3] either by increasing the thermoelectric power-factor (σS^2)[4,5] or by decreasing thermal conductivity.[6] In the current manuscript, we investigate the possibility of the former.

Hicks and Dresselhaus proposed to use quantum size effects in low-dimensional materials to create sharp features in the density-of-states and enhance the Seebeck coefficient.[7] Recently giant Seebeck coefficients have been achieved using high-density two-dimensional electron gas.[8] However, the issue of the normalization by the electron confinement region rather than the atomic size of the dopants needs to be clarified.[9] Introducing resonant energy levels of doped impurities into the bulk band-structure also modifies the density of states and therefore the Seebeck coefficient.[10] On the other hand, one can create sharp features in the relaxation time in a material with metallic-like density of states, by introducing potential scattering at heterointerfaces.[11,12] This also leads to the enhanced Seebeck coefficient. Poudel et al[13] demonstrated that by nanostructuring, enhancement in the power factor and reduction in the thermal conductivity are achievable simultaneously, resulting in significant enhancement in the thermoelectric figure-of-merit. Nanoparticles can have several effects on electrical properties. First, they can contribute free electrons/holes to the host matrix (leading to ionized nanoparticles). Second, they introduce variations in conduction/valence band edge since there may be a band offset between nanoparticles and the host besides the Coulomb potential of the ionized particles. These variations in potential would make the effective band-structure different from that of the host matrix. Finally, the potential randomness from nanoparticle size and spatial variation would scatter electrons and therefore reduce the electron momentum relaxation time. It is a big challenge to simulate the influence of nanoparticles on electron transport accurately because of their random spatial and size distributions. A common approach is to assume that electrons are transported in the host matrix but with reduced mobility due to a series of independent nanoparticle scattering events.[14,15] Such a treatment is valid only when the volume concentration of nanoparticles is less than a few percent.[16] At higher concentrations, coherent multiple scatterings are possible and transport properties of nanoparticles become important since carriers spend a considerable amount of their time inside nanoparticles. For example, in pure GaAs the electron mean free path at room temperature is more than 30 nm and it reaches several micrometers at low temperatures. However, the average distance between nanoparticles is about 5.4 nm when their volume fraction is 5% and their average radius is 1 nm. A better approach is to average over nanoparticles and the host

* To whom correspondence should be addressed. E-mail: ali@soe.ucsc.edu.
Received for review: 10/12/2010
Published on Web: 12/09/2010

DOI: 10.1021/nl103581z | *Nano Lett.* **2011,** *11,* 225–230

matrix[17] to obtain the effective band structure and the momentum relaxation time. The band-structure modifications are particularly important if nanoparticles could introduce sharp features in the differential conductivity. It has been shown that Tl impurities can create peaks in the valence band density-of-states of lead telluride.[18] Similar peaks might be created by nanoparticles. The coherent potential approach (CPA) provides a framework that can include the band structure modifications as well as the relaxation time changes by averaging over nanoparticles and host media.[19] It has been very successful in describing electronic properties of metallic alloys.[20] CPA takes into account electron multiple scatterings as well as nanoparticle transport properties, which are important for samples with relatively high volume fraction of nanoparticles (>1%). For smaller concentration of nanoparticles, scattering events become independent and the CPA converges to the partial wave method,[21] which was previously used to explain the electrical conductivity and the Seebeck coefficient of InGaAlAs samples with 0.3−0.6% volume fraction of ErAs nanoparticles.[22]

In this paper, we use the previously developed CPA formalism to optimize the power factor at each temperature for various nanoparticle concentrations. We study the effect of the nanoparticle size distribution as well as the optimum doping. In what follows, we describe the model and the optimization procedure, followed by a discussion of the results. In the first part of the paper, we choose a constant scattering rate for all other scattering mechanisms and a step potential for nanoparticles to get some intuition for the best size distribution of nanoparticles. We then use the optimized nanoparticle distribution and apply the formalism to a real host material (GaAs), in which we consider all of the important scattering mechanisms and their energy dependence, as well as band-bending in the nanoparticle step potential due to the screened Coulomb effect.

Assume G_0 is the electron Green's function of the homogeneous system. Introducing a nonuniform potential V of nanoparticles to the system will modify the Green function to $G^{-1} = G_0^{-1} - V$. Dealing with the exact $G(\omega, r, r')$ is complicated not only because of its complicated form but also because it contains too much information and it is hard to extract useful data out of it. Instead, we consider its value averaged over different configurations of random potential profiles $\langle G\rangle_c$. The self-energy is then defined as $\langle G\rangle_c^{-1} = G_0^{-1} - \Sigma$. While V is the potential of an exact configuration, Σ is a nonlocal operator, which does not depend on any particular configuration but on the statistical characteristics of the random assemble. If Σ does not have any k-dependence, then we can define a renormalized effective medium, with the self-energy $\Sigma(E)$ added to the host Hamiltonian. Its effect is to shift the electron energy and give it a finite lifetime through its imaginary part. The CPA condition states that the real part of the average T-matrix $\langle T\rangle_c$ in the effective medium and in the forward direction is zero.[23,24] Following the work

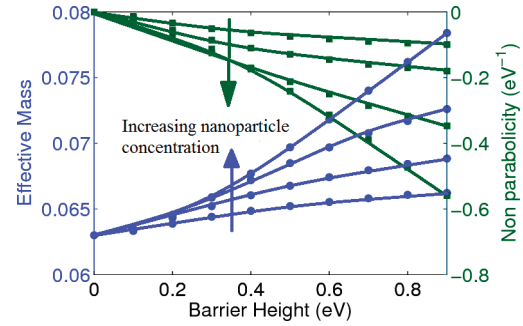

FIGURE 1. Modifications of the band structure versus band-offset between nanoparticles and the host (barrier height) for different volume fractions of nanoparticles (1,2,5, and 10%). Circles (left axis): effective mass in the presence of nanoparticles. In this case (positive barrier height), effective mass increases compared to the host matrix. Squares (right axis): the nonparabolicity parameter (α defined by $E(1 + \alpha E) = \hbar^2k^2/2m^*$). A Gaussian radii distribution centered at 2 nm with variance 0.1 nm was assumed for spherical nanoparticles with a step barrier potential inside a host matrix with parabolic band dispersion (effective mass of 0.063).

of Sheng,[25,26] we assume each nanoparticle is a sphere embedded inside another bigger sphere, which represents the host matrix, and both spheres are placed inside the effective medium. A discrete size distribution is assumed for the nanoparticles. The t-matrix of each size is calculated by solving the Schrödinger equation inside the spheres (using the shooting method[27]) and matching the slope of the wave function with the analytical solutions of the effective medium at the outer interfaces. Here small t refers to a single-particle configuration and capital T refers to the total T-matrix. We assume $\langle T\rangle_c \sim \Sigma_i n_i \langle t\rangle_i$, where i is the index labeling individual single-particle configurations and n_i is the concentration of each configuration. The solutions of the CPA equation at each energy ($Re(\Sigma_i n_i \langle k_e|t|k_e\rangle_i) = 0$) define the effective band structure. The scattering amplitude can also be calculated from the T-matrix ($f(k'_e,k_e) = -\langle k'_e|t|k_e\rangle/4\pi$). Finally knowing the band structure and the scattering rate, thermoelectric properties can be calculated using the linear Boltzmann integrals.[28]

We start from a simple case described in the following. A parabolic band-structure is assumed for the host matrix and nanoparticles have the same effective mass as that of the host. The particle potential is a step function whose height represents the band-offset between the host matrix and the nanoparticle. In a first instance, a constant scattering rate is considered for the sum of all other scatterings. A Gaussian distribution was assumed for the nanoparticle sizes. Under these assumptions, the calculations show that for step barriers, the effective band-structure has an upward energy shift relative to the host matrix and nonparabolic dispersion relation ($E(1 + \alpha E) = h^2k^2/2m^*$) is created. Figure 1 shows that the effective mass can be increased by up to 20% when the nanoparticle percentage is as high as 10% and the band-offset is as high as 0.8 eV. The nonparabolic parameter is negative for all nanoparticle concentrations and barrier heights that were studied. This means that low-

DOI: 10.1021/nl103581z | *Nano Lett.* **2011,** *11,* 225–230

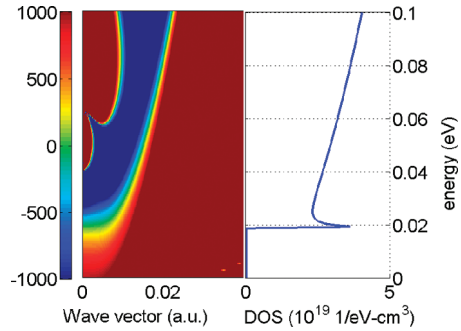

FIGURE 2. The effective band structure of a step well. Well depth is −0.6 eV and volume fraction is 1%. Other properties are the same as Figure 1. Left: color axis is the real part of the average *T*-matrix. The *y*-axis is the energy axis (this axis is shared between the plots) and *x*-axis is the effective wave vector in atomic units. Zero contours of this plot define the effective band dispersion. Note that there are some unphysical roots deeper in the band, which are disregarded in the formalism. Right plot: *x*-axis is the density of states, which has a peak due to resonant levels of nanoparticles.

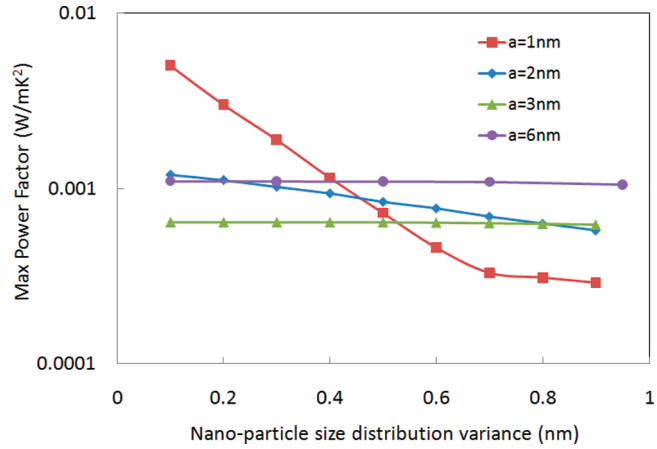

FIGURE 3. Maximum power factor versus nanoparticle size variance. Different curves refer to different average radius (a) of nanoparticles. In this curve, we assumed a 5% nanoparticle volume fraction and 0.5 eV nanoparticle barrier height.

energy electrons are slowed down while high energy ones are not affected as much. For step wells, the dispersion curve is changing significantly as a function of the well depth. For shallow wells, the conduction band is shifting down with no significant change, just like step barriers. However, at larger band offsets, the dispersion curve has changes that are more significant; it shifts upward and flattens at the bottom of the conduction band. This is a result of resonance of incident electrons off the weakly bound states of the well. Such a dispersion results in a peak in the density of states as shown in Figure 2.

Incorporation of nanoparticles gives additional freedom in the optimization of thermoelectric properties. A set of parameters are related to the nanoparticle size distribution. If all nanoparticles have the same size, there are two advantages for electron transport. The first is that since the randomness of the system is reduced, scattering rates are smaller and electrons can move more freely (higher mobility). Second, the differential conductivity has sharper features as a function of electron energy. There is less smearing because of nanoparticle size variations. This in turn could lead to higher Seebeck coefficients and thus higher thermoelectric power factors. To investigate the effects of nanoparticle size distribution, we changed the variance of the distribution and scanned the power factor at different Fermi-levels. A Gaussian distribution is assumed for the nanoparticle sizes. Two conditions are enforced on the discrete Gaussian distribution. First, the radii and their weight should be positive and second, the discretized distribution should be symmetric around its center (average nanoparticle size). The temperature is set at 300 K and the barrier height 0.5 eV. To see nanoparticle effects more clearly, a relatively smaller constant scattering rate of 10^{12} s^{-1} is chosen for other scattering mechanisms. Figure 3 shows the thermoelectric power factor maximized with the Fermi level, which decreases when the size variance increases. This dependence is more prominent for smaller nanoparticles. For nanoparticle radii larger than 3 nm, the maximum thermoelectric power factor is almost independent of nanoparticle size dispersion.

Figure 3 indicates that samples with high volume fraction of small nanoparticles (∼1 nm in radius) with small variations in their sizes have the potential to enhance the power factor. One should note that the band structure and the electron-nanoparticle scattering rate are independent of the temperature under the assumption that the potential barrier is fixed. The temperature plays a role in that it defines a Fermi-window for electron transport. At low temperatures, the Fermi window is narrow and it can catch sharp features of density of states or scattering rates. Thus, the enhanced thermoelectric power factor could be observed. In the absence of such sharp features, overall trends stay the same at different temperatures. The thermoelectric power factor enhancement is largest when there are no other scatterings except for ionized impurity scattering or ionized nanoparticle scattering. To illustrate the advantage of the suggested nanoparticle configuration (high concentration of uniform small nanoparticles), we chose a binary semiconductor, GaAs, where there is no alloy scattering, the mass is isotropic, and scattering parameters are very well characterized. This allows us to make quantitative predictions about the potential enhancement in the power factor. In cases where additional scatterings are present, the enhancement is lower. In GaAs, the only important scatterings are phonons and impurities and the former can be reduced significantly by going to low temperatures. One should note that nanoparticles are not always better than ionized impurities. In most thermoelectrics, the optimum Fermi-level is close to the conduction band-edge. Near the conduction band, ionized impurity rates versus energy displays a sharp slope (see Supporting Information) and this results in large Seebeck coefficients while nanoparticles, mainly because of their large size variations, do not have such sharp features. Here we try to find specific conditions under

DOI: 10.1021/nl103581z | *Nano Lett.* **2011,** *11,* 225–230

which nanoparticle doping can improve the thermoelectric power factor significantly.

Up to now, we have not considered the doping effect of nanoparticles. If nanoparticles contribute free electrons to the matrix, they will hold net charges and there will be band bending at the interface of nanoparticle and host matrix. The screened Coulomb potential of nanoparticles is similar to that of ionized impurities and would significantly change the effective band structure and momentum relaxation time under the CPA framework. After including the corrected nanoparticle potential, one can make a fair comparison between impurity-doped and nanoparticle-doped materials. For simplicity, a single valley parabolic band-structure for GaAs is assumed with an effective mass of 0.063 m. We use the relaxation time approximation and add polar optical phonons and acoustic phonons together with impurity/nanoparticle scattering rates. Two samples are considered: the first sample is impurity doped. For this sample, we assume that there is a small bonding energy (ε_d) of 2 meV and impurities are ionized with a probability of $\exp(-\varepsilon_d/k_BT)$. Both ionized and neutral impurity scatterings are included. The second sample is nanoparticle doped. A relatively high volume fraction of 5% is assumed with the band offset of 0.2 eV and an average radius of 1 nm. The variance of nanoparticle size distribution was assumed to be small (0.1 nm) and therefore the particles do not reduce the mobility as much as a broad distribution would. Free electrons in the conduction band are assumed to come only from nanoparticles. The average number of electrons per nanoparticle was calculated for each specific carrier density. We assumed a uniform carrier density inside nanoparticles to calculate the band bending at the interfaces of nanoparticles and host matrix.[22] In practice, for example, various metallic and semimetallic rare earths can be embedded inside III−V semiconductors to tune the band offset. In the modeling, we scanned the carrier density to calculate the maximum power factor for each sample. Figure 4 shows the results at room temperature. Details of scattering rates are provided in the Supporting Information. It shows that with replacing the impurities by ionized nanoparticles, the power factor can be enhanced at room temperature by 50%. The main advantage of nanoparticles compared to impurities in this case is that the charge is not localized at the center but rather distributed over a finite volume. If the volume fraction is large enough and the nanoparticles are small enough, the average number of free electrons coming from nanoparticles can be small, resulting in small band bending and lower electron scattering rate.

We note that there is a slight reduction in the Seebeck coefficient of the nanoparticle-doped sample compared to the impurity-doped one when the Fermi level is close to the band edge. However, the enhanced mobility dominates and overall the thermoelectric power factor is increased. The improvement in power factor could be large since doping via embedded nanoparticles of small and uniform size can reduce electron mobility much less than the doping via traditional impurity scattering. Thus, one can achieve high electrical conductivities while maintaining a large Seebeck coefficient. The thermoelectric power factor enhancement is more prominent at lower temperatures. This is due to lower phonon scattering rates and relatively higher ratio of impurity/nanoparticle scatterings. Figure 5 summarizes the results at different temperatures. At each temperature, we optimized the thermoelectric power factor of each sample with respect to the Fermi level (similar to what is done in Figure 4). We noted that the optimum Fermi-level (where the power factor is maximized) for nanoparticle-doped sample is higher than that of the impurity-doped sample, resulting in a higher electrical conductivity.

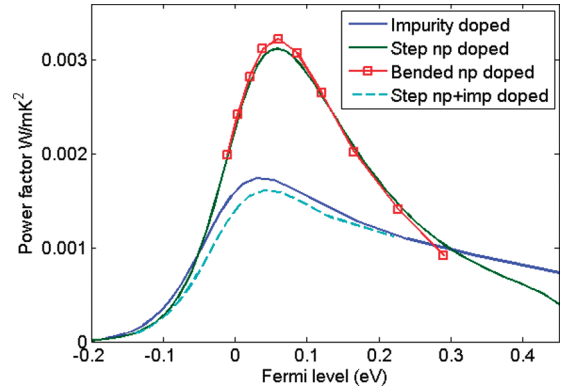

FIGURE 4. Thermoelectric power factor versus Fermi level at room temperature for nanoparticle doped GaAs compared to that for impurity doped GaAs in several cases. Solid blue line, impurity doped sample; solid green line, nanoparticle doped sample (step barriers considered, band-bending was not included); red squares, nanoparticle doped samples taking into account the band-bending; and dashed blue line, nanoparticle sample in which electrons are assumed to come from impurities and thus impurity scattering dominates the mobility.

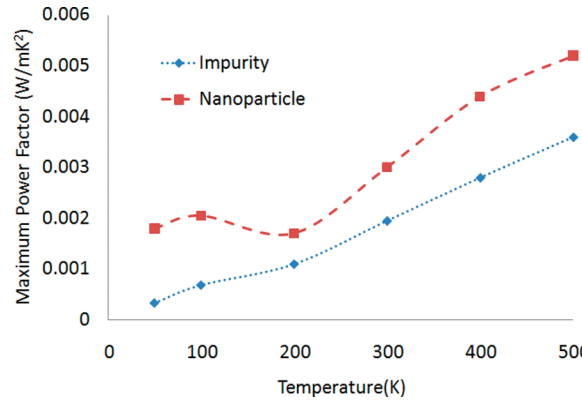

FIGURE 5. Maximum thermoelectric power factor versus temperature for the nanoparticle-doped GaAs compared to the impurity-doped GaAs. At each temperature, the power factor was maximized versus Fermi-level. Modeling is performed for GaAs with 5% volume fraction of 0.2 eV height nanoparticles. Band bending of the nanoparticles are included. Phonon scattering rates (polar optical and acoustic) are also included in the calculations. Refer to text for other properties.

DOI: 10.1021/nl103581z | *Nano Lett.* **2011,** *11,* 225–230

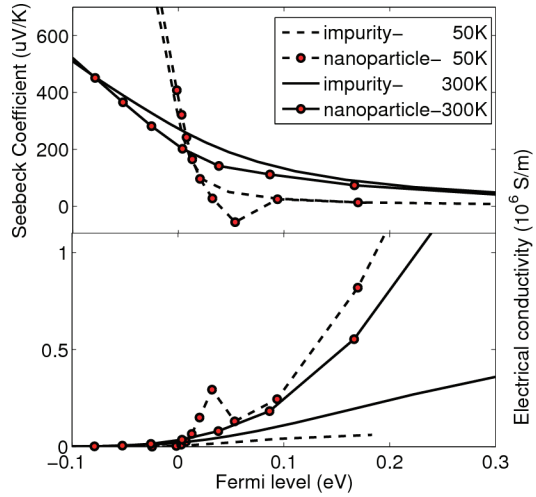

FIGURE 6. Seebeck coefficient (top) and electrical conductivity (bottom) versus Fermi level for impurity and nanoparticle doped samples at 50 and 300 K. Samples are described in the text.

We further noted that unlike room temperature, at low temperatures, the Seebeck coefficient is enhanced at the optimum Fermi level. Figure 6 shows the Seebeck coefficient and the electrical conductivity versus Fermi-level at 50 and 300 K for nanoparticle-doped and impurity-doped samples. The observed peak/dip in the electrical conductivity/Seebeck at 50 K is due to the presence of nanoparticles, which introduce a peak in the density of states very close to the bottom of the conduction band as illustrated in Figure 2. As the Fermi-level scans through the peak in the density of states, the Seebeck coefficient sign is changed. This peak results in an enhancement of the Seebeck coefficient at Fermi levels several K_BT below the peak. Both the enhanced Seebeck and electrical conductivity make the thermoelectric power factors larger at low temperatures. The peak in the electrical conductivity cannot be seen at high temperatures (Figure 6, 300 K) where it is washed out by the large Fermi window. However, mobility enhancement still increases the power factor.

One should note that dispersion curves and therefore differential conductivities of the nanoparticle-doped sample depend on the Fermi level. In fact, since the number of ionized carriers per nanoparticle increases as the Fermi level increases, the band bending profile at the interface of the nanoparticle and host matrix increases, resulting in the possibility of bound states. These bound states can act as resonant levels and introduce peaks in the density of states at some specific Fermi levels. The position of the peak changes as the Fermi level changes. However, at the end it results in a wide single peak in the electrical conductivity versus Fermi level curve.

In summary, we used the coherent potential approximation to investigate thermoelectric transport properties of nanoparticle-doped materials. At low concentrations, it recovers the results of the partial wave method for single particle scattering. At higher concentrations, it includes multiple scatterings and transport properties of nanoparticles and therefore gives the effective band dispersion and relaxation times more accurately. If there are any sharp features in the density of states of the nanocomposite, this method is capable of capturing that, while partial wave/Born cannot. Within a simple model of step function barriers/wells inside a host matrix with parabolic band, the effective band structure shifts up/down and nonparabolic band dispersion with modified effective mass is created. Deep step wells can introduce resonant states and therefore sharp features in the density of states. Nanoparticles are not always better than ionized impurities. In this paper, we found the conditions under which nanoparticles can improve the thermoelectric power factor significantly. We showed that relatively high concentration of small, uniform size nanoparticles inside semiconductors in which electron mobility is mainly limited by ionized impurity scattering is the key requirement. The enhancement is largest at low temperatures for the case of GaAs since electron mobility is dominated by polar optical phonons at higher temperatures. Nanoparticles of uniform size have an advantage since they do not reduce electron mobility as much. Uniform nanoparticles introduce a peak in the density of states. In the current study, the peak is very close to the conduction band edge and results in thermoelectric power factor enhancement. The peak is observable in the electrical conductivity/Seebeck coefficient at low temperatures but is smeared out at high temperatures (Figure 6). Compared to impurity-doping, the electrical conductivity of the nanoparticle-doped sample is enhanced at all Fermi-levels, which is mainly from the mobility increase. The Seebeck coefficient is reduced for most doping values and is enhanced in a narrow range of Fermi levels near the band edge. At low temperatures, the optimum Fermi-level shifts to lower values at which the Seebeck coefficient enhancement can be seen. The enhancements of both Seebeck coefficient and electrical conductivity result in a significant increase in the thermoelectric power factor by 450% at 50 K.

Acknowledgment. This work was supported by ONR MURI Thermionic Energy Conversion Center and DARPA NMP program.

Supporting Information Available. Scattering rates, table of GaAs material parameters, and additional figures. This material is available free of charge via the Internet at http://pubs.acs.org.

REFERENCES AND NOTES

(1) Rowe, D. M. *Thermoelectrics Handbook, Macro to nano*; CRC press, Taylor & Francis: Boca Raton, FL,2006.
(2) Deng, Y.; Nan, C. W.; Wei, G. D.; Guo, L.; Lin, Y. H. *Chem. Phys. Lett.* **2003**, *347*, 410.
(3) Urban, J. J.; Talapin, D. V.; Shevchenko, E. V.; Kagan, C. R.; Murray, C. B. *Nat. Mater.* **2007**, *6*, 115.
(4) Zide, J. M. O.; Klenov, D. O.; Stemmer, S.; Gossard, A. C.; Zeng, G.; Bowers, J. E.; Vashaee, D.; Shakouri, A. *Appl. Phys. Lett.* **2005**, *87*, 112102.

DOI: 10.1021/nl103581z | *Nano Lett.* **2011,** *11,* 225–230

(5) Dirmyer, M. R.; Martin, J.; Nolas, G. S.; Sen, A.; Badding, J. V. *Small* **2009**, *5*, 933–937.
(6) Kim, W.; Singer, S. L.; Majumdar, A.; Zide, J. M. O.; Klenov, D.; Gossard, A. C.; Stemmer, S. *Nano Lett.* **2008**, *8*, 2095.
(7) Hicks, L. D.; Dresselhaus, M. S. *Phys. Rev. B* **1993**, *47*, 12727.
(8) Ohta, H.; Kim, S.; Mune, Y.; Mizoguchi, T.; Nomura, K.; Ohta, S.; Nomura, T.; Nakanishi, Y.; Ikuhara, Y.; Hirano, M.; Hosono, H.; Koumoto, K. *Nat. Mater.* **2007**, *6*, 129.
(9) Vineis, C. J.; Shakouri, A.; Majumdar, A.; Kanatzidis, M. G. *Adv. Mater.* **2010**, *22*, 3970–3980.
(10) Heremans, J. P.; Jovovic, V.; Toberer, E. S.; Saramat, A.; Kurosaki, K.; Charoenphakdee, K.; Yamanaka, S.; Snyder, J. F. *Science* **2008**, *321*, 554.
(11) Shakouri, A.; Bowers, J. E. *Appl. Phys. Lett.* **1997**, *71*, 1234–1236.
(12) Shakouri, A.; Zebarjadi, M. In *Thermal Nanosystems and Nanomaterials*; Volz, S., Ed.; Springer: Berlin, 2009; Vol. *118*, p 225.
(13) Poudel, B.; Hao, Q.; Ma, Y.; Lan, Y. C.; Minnich, A.; Yu, B.; Yan, X.; Wang, D. Z.; Muto, A.; Vashaee, D.; Chen, X.; Liu, J. M.; Dresselhaus, M. S.; Chen, G.; Ren, Z. F. *Science* **2008**, *320*, 634.
(14) Minnich, A. J.; Lee, H.; Wang, X. W.; Joshi, G.; Dresselhaus, M. S.; Ren, Z. F.; Chen, G.; Vashaee, D. *Phys. Rev. B* **2009**, *80*, 155327.
(15) Faleev, S. V.; Leonard, F. *Phys. Rev. B* **2008**, *77*, 214304.
(16) Zebarjadi, M.; Esfarjani, K.; Shakouri, A.; Bian, Z. X.; Bahk, J. H.; Zeng, G. H.; Bowers, J. E.; Lu, H.; Zide, J. M. O.; Gossard, A. C. *J. Electron. Mater.* **2009**, *38*, 954.
(17) Bergman, D. J.; Levy, O. *J. App. Phys.* **1991**, *70*, 6821–6833.
(18) Nemov, S. V.; Ravich, Y. I. *Phys.-Usp.* **1998**, *41*, 735.
(19) Lax, M. *Rev. Mod. Phys.* **1951**, *23*, 287.
(20) Velicky, B. *Phys. Rev.* **1969**, *184*, 614.
(21) Schiff, L. I. *Quantum Mechanics*; McGraw-Hill Book Company: New York, 1949.
(22) Zebarjadi, M.; Esfarjani, K.; Shakouri, A.; Bahk, J. H.; Bian, Z. X.; Zeng, G. H.; Bowers, J.; Lu, H.; Zide, J.; Gossard, A. C. *Appl. Phys. Lett.* **2009**, *94*, 202105.
(23) Soven, P. *Phys. Rev.* **1967**, *156*, 809.
(24) Velicky, B.; Kirkpatr, S.; Ehrenrei, H. *Phys. Rev.* **1968**, *175*, 747.
(25) Sheng, P. *Philos. Mag. B* **1992**, *65*, 357.
(26) Sheng, P. *Introduction to Wave Scattering, Localization, and Mesoscopic Phenomena*; Academic Press: New York, 1995.
(27) Stoer, J.; Bulirsch, R. *Introduction to Numerical Analysis*; Springer-Verlag: New York, 1980.
(28) Marder, M. P. *Condensed Matter Physics*; John Willey & Sons Inc.: New York, 2000; Chapter 17.

DOI: 10.1021/nl103581z | *Nano Lett.* **2011,** *11,* 225–230